THE ASTROPHYSICAL JOURNAL, 456:163–173, 1996 January 1

HIGH-RESOLUTION *IRAS* MAPS AND INFRARED EMISSION OF M31. II. DIFFUSE COMPONENT AND INTERSTELLAR DUST

CONG XU
Max-Planck-Institut für Kernphysik, Postfach 103980, 69117 Heidelberg, Germany
AND
GEORGE HELOU
IPAC 100-22, California Institute of Technology, Pasadena, CA 91125
Received 1994 May 9; accepted 1995 July 6

ABSTRACT

Large-scale dust heating and cooling in the diffuse medium of M31 is studied using the high-resolution (HiRes) *IRAS* maps in conjunction with UV, optical (*UBV*), and H I maps. A dust heating/cooling model is developed based on a radiative transfer model which assumes a "sandwich" configuration of dust and stars and takes fully into account the effect of scattering of dust grains. The model is applied to a complete sample of "cells" (small areas of size $2' \times 2'$) generated from the above maps. The sample covers the M31 disk in the galactocentric radius range 2–14 kpc and includes only the cells for which the contribution of the discrete sources to the 60 μm surface brightness is negligible (<20%). This effectively excludes most of the bright arm regions from our analysis. We find the following:

1. The mean optical depth (viewed from the inclination angle of 77°) increases with radius from $\tau_v \sim 0.7$ at $r = 2$ kpc outward, reaches a peak of ~ 1.6 near 10 kpc, and stays quite flat out to 14 kpc, where the signal falls below the 5 σ level.
2. A correlation between τ_v and H I surface density is suggested by the similarity between their radial profiles. Significant differences are found between the radial profiles of the H_2 gas (estimated from CO) and of the dust (from τ_v), which are most probably caused by the large uncertainty in the CO-to-H_2 conversion factor, and to the underrepresentation of H_2-rich regions in the sample of cells of *diffuse* regions.
3. The τ_v/N(H I) ratio decreases with increasing radius in the disk of M31, with an exponential law fit yielding an e-folding scale length of 9.6 ± 0.4 kpc.
4. The optical depth adjusted for this gradient, $\tau_{v,c}$, is strongly and linearly correlated with N(H I) over 1.5 orders of magnitude of column density, indicating that at a given radius r the dust column density is proportional to the H I gas column density, with the proportionality factor decreasing with increasing r.
5. With the assumption that the ratio of τ_v to dust column density is the same as that in the solar neighborhood, the portion of the M31 disk at radii between 2 and 14 kpc contains $1.9 \pm 0.6 \times 10^7\ M_\odot$ of dust, yielding a global dust–to–total gas mass ratio of $9.0 \pm 2.7 \times 10^{-3}$, very close to solar neighborhood value.
6. The nonionizing UV radiation, mainly caused by B stars (4–20 $M_\odot$), contributes only 27% of the heating of the diffuse dust in M31. Throughout the M31 disk, heating of the diffuse dust is dominated by optical radiation from stars at least a billion years old.

Subject headings: diffuse radiation — dust, extinction — galaxies: individual (M31) — galaxies: ISM — galaxies: photometry — infrared: galaxies

1. INTRODUCTION

This is the second paper in a series on the infrared (IR) emission of the Andromeda galaxy (M31) studied using the new high-resolution (HiRes) *IRAS* maps. In the first paper (Xu & Helou 1996, hereafter Paper I) we studied the overall morphology and the discrete sources of the far-infrared (FIR) emission in the disk of M31. In this paper we investigate the diffuse FIR component and the properties of the interstellar dust in M31.

M31 is an ideal target for studies of the FIR emission of the diffuse interstellar dust *not* associated with star formation regions in a galaxy other than the Milky Way. First of all, being the nearest spiral outside the Milky Way, M31 is well resolved by *IRAS*. Thus, the discrete sources, which represent most of the FIR emission associated with star formation regions (Paper I) can be distinguished from diffuse emission. Second, because M31 has a very low present-day star formation rate, about an order of magnitude lower than that of the Milky Way (Walterbos 1988; Paper I), the diffuse component dominates the FIR emission of M31, whereas the dust associated with H II regions contributes only 30% ± 14% of the total IR luminosity of M31 (Paper I).

It has been well established that the diffuse FIR emission in a galaxy is caused by the thermal radiation of the interstellar dust heated by the interstellar radiation field (Jura 1982; Cox, Krügel, & Mezger 1986; Helou 1986; Lonsdale-Persson & Helou 1987; Xu & De Zotti 1989). The diffuse FIR emission has been widely used to study the properties of the interstellar dust, e.g., abundance of dust, dust-to-gas ratio, composition and size distribution of dust grains, heating and cooling of dust grains, etc. (Draine & Anderson 1985; Walterbos & Schwering 1987, hereafter WS87; Désert, Boulanger, & Puget 1990). Xu & Helou (1994) studied the *IRAS* color-color diagrams of the diffuse component in the M31 disk, and they found rather low $I_{60\mu m}/I_{100\mu m}$ ratios and high $I_{12\mu m}/I_{25\mu m}$ ratios for those regions in which the interstellar radiation field (ISRF) is low.

This was interpreted as evidence of deficiency of very small grains (but not polycyclic aromatic hydrocarbons [PAHs]) in the M31 disk. In this paper we attempt to answer the following questions:

1. How is the interstellar dust distributed in M31? How does it correlate with H I gas and H_2 gas?
2. How much interstellar dust does M31 have? What is the dust-to-gas ratio?
3. What is the energy budget of the diffuse interstellar dust?

In the literature, the most common approach for studying the abundance and the distribution of dust using its FIR emission is based on the assumption that the dust is in thermal equilibrium with a characteristic temperature T_d (see the review by Soifer, Houck, & Neugebauer 1987). Then the amount of the dust may be estimated from the infrared optical depth defined by $\tau_\lambda = I_\lambda / B_\lambda(T_d)$ (WS87; Deul 1989). There are two problems with this approach: (1) If there are several temperature components sampled along the line of sight, as is likely, the characteristic temperature is biased to the highest values because of the strong dependence of the emission on temperature (WS87); (2) the assumption that the dust responsible for the FIR emission is in thermal equilibrium may not be valid because, particularly in the low ISRF regions, a substantial part of the FIR emission detected by *IRAS* may be caused by grains undergoing temperature fluctuations (Désert et al. 1990). These two biases both tend to overestimate the emissivity and, consequently, underestimate the dust abundance. As a consequence, the dust-to-gas ratio resulting from such an approach is usually on the order of 10^{-3} (Devereux & Young 1990), about an order of magnitude lower than the canonical value estimated from optical studies (Savage & Mathis 1979; van den Bergh 1975).

In this paper we develop a dust heating and cooling model which takes a different approach. The model is based on the assumption that the interstellar dust is heated by the nonionizing UV (912–3650 Å) and the optical (3650 Å–9000 Å) radiation in the interstellar radiation field (ISRF) and cools down by infrared radiation (8–1000 μm). In other words, the model treats dust grains as "frequency converters" which convert the UV and optical radiation to FIR radiation via the absorption-reradiation process. It is from the fraction so converted rather than from the emission alone that we estimate the optical depth of the disk, i.e., the column density of dust. Thus, no assumption about the dust thermal equilibrium and T_d is needed. By adopting an empirical extinction curve of M31 (Hutchings et al. 1992; Walterbos & Kennicutt 1988), our model is also insensitive to the grain model (i.e., the composition and the size distribution of dust grains). Quantitatively, our model is based on a radiative transfer code which takes the observed intensities of the FIR, UV, and optical emissions as input. It then estimates (1) the optical depth of the disk which can be converted to dust column density, (2) the amount of heating of dust attributable to the nonionizing UV and to the optical radiation, respectively, and in principle (3) the extinction-corrected surface brightness of the UV and optical radiation at different wavelengths.

In § 2 we describe the data. The model for the heating and cooling of interstellar dust is presented in § 3. The results are given in § 4. A discussion is carried out in § 5. Section 6 contains the summary. As in Paper I, we assume for M31 a distance of 690 kpc (1′ = 200 pc along the major axis), an inclination angle of $i = 77°$ ($i = 0$ for face-on), and P.A. = 37°.

2. THE DATA

We define the diffuse FIR component as the emission from interstellar dust not associated with H II regions. Sources at 60 μm (Xu & Helou 1993; Paper I) are used to represent the dust emission associated with H II regions. In order to distinguish regions in which the sources dominate from those in which the diffuse emission dominates, we break the M31 field into small "cells," each of size 2′ × 2′, corresponding to a linear size of 0.4 × 1.8 kpc^2 in the plane of M31. Point-by-point studies are made on these cells. The HiRes maps as well as a UV (2030 Å) photometry map (Milliard 1984), which has an angular resolution of about 1.5, three optical (*UBV*) photometry maps (Walterbos & Kennicutt 1987) of resolution ~15″, and an H I map (Brinks 1984; Brinks & Shane 1984) of resolution of 48″ × 72″, are smoothed to a common 1.7 (HPBW) round beam on a grid with 0.5 pixels. A complete sample of the M31 cells is constructed with these maps, with the surface brightness of each cell taken from the corresponding map by averaging the surface brightness of a 4 × 4 array of adjacent pixels (Xu & Helou 1994). Cells are included only if:

1. both the 60 μm and 100 μm surface brightness exceed a signal-to-noise ratio of 5;
2. the contribution from the FIR sources is neglible, namely, $Q_s = I_{60\,\mu m,s}/I_{60\,\mu m} \leq 0.2$, where $I_{60\,\mu m,s}$ is being the contribution of the sources to the 60 μm surface brightness taken from the source map (Xu & Helou 1993) and $I_{60\,\mu m}$ is the total 60 μm surface brightness;
3. they are not located in the optical bulge, which is the central ellipse of size 12′ × 20′ (Walterbos & Kennicutt 1988, hereafter WK88).

The sample contains 358 such cells.

It should be noted that the 60 μm source map (Xu & Helou 1993) includes all the 70 sources extracted using the Gaussian fitting procedure with the size of fitting area of 4.5 × 4.5. As pointed out in Paper I, these sources suffer confusion problems, and 16 of them have not been included into the final list of sources in Paper I. On the other hand, the sources underrepresent the emission of the H II region–associated dust (Paper I); hence, some cells in the sample may be contaminated by the large contribution from this dust. Nevertheless, these uncertainties will have little effect on our conclusions on the diffuse dust, since our analysis is based on statistics of a large sample of cells, most of which are likely to be dominated by the true diffuse component.

3. MODEL FOR DUST HEATING AND COOLING

Applied to each cell (2′ × 2′) in the M31 disk, the model takes as input from the observed intensities of the optical, UV, and FIR emissions, and gives as output the optical depth to V-band (5500 Å) radiation τ_v by solving the radiative transfer equation. The model also estimates the amount of dust heating caused by the UV-optical radiation at different wavelengths. The optical depths to radiation at wavelengths other than 5500 Å can be estimated from τ_v using the adopted extinction curve given in Table 1.

The radiative transfer model is based upon the algorithm developed by van de Hulst & de Jong (1969), which takes the effect of scattering fully into account in the sense that scattered light of any order has been calculated using an iteration procedure from lower order scattered light. An infinite-plane-parallel geometry for the radiative transfer problem is adopted.

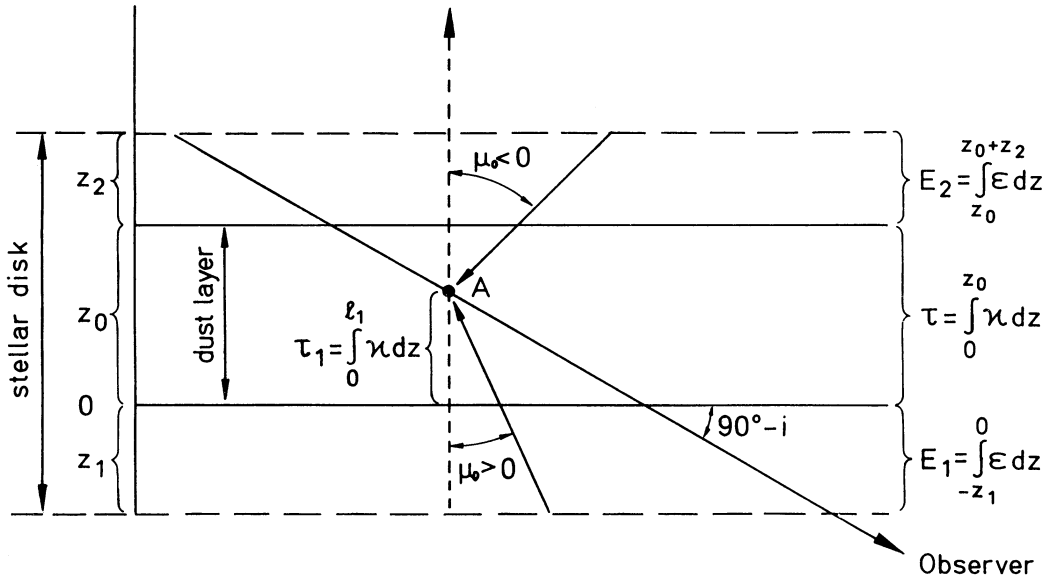

FIG. 1.—Schematic illustration of definitions of several parameters used in the dust heating model: ϵ denotes the volume emissivity, κ is the volume absorptivity, $\mu_0 = \cos(i_0)$, and $\tau_1 = \int_0^{l_1} \kappa\, dz$.

In contrast with van de Hulst & de Jong (1969), we allow for different thicknesses of the star layer and dust layer. A "sandwich" configuration (Fig. 1) is used for the dust and star distributions in a galaxy disk with the scale height of the stars assumed to be larger than or equal to that of the dust.

Following van de Hulst & de Jong (1969), the direct star light is defined as of zeroth order:

$$I_0(\tau_1, \mu_0) = \begin{cases} S_0(1 - e^{-\tau_1/\mu_0}) + \dfrac{E_1}{\mu_0} e^{-\tau_1/\mu_0} & (\mu_0 > 0)\,, \\ S_0[1 - e^{-(\tau-\tau_1)/(-\mu_0)}] - \dfrac{E_2}{\mu_0} e^{-(\tau-\tau_1)/(-\mu_0)} & (\mu_0 < 0)\,, \end{cases} \quad (1)$$

where I_0 is the zero-order intensity seen at a point (e.g., A in Fig. 1) in the plane toward direction $\mu_0 = \cos(i_0)$, and

$$E_1 = \int_{-z1}^{0} \epsilon\, dz \quad (2)$$

is the integral of the emissivity ϵ over the layer of stars lying in front of the dust layer, and

$$E_2 = \int_{z0}^{z0+z2} \epsilon\, dz \quad (3)$$

is the integral of the emissivity over the layer of stars lying behind the dust layer. The zero-order source density S_0 is assumed constant within the dusty layer. The definitions of μ_0, τ_1, τ, z_0, z_1, and z_2 are illustrated in Figure 1. The first and higher order scattered radiation can be calculated as follows:

$$I_n(\tau_1, \mu_n) = \begin{cases} \displaystyle\int_{\tau_1}^{\tau} S_n(\tau', \mu_n) e^{(\tau_1-\tau')/(-\mu_n)} \frac{d\tau'}{-\mu_n} & (\mu_n < 0)\,, \\ \displaystyle\int_{0}^{\tau_1} S_n(\tau', \mu_n) e^{(\tau'-\tau_1)/\mu_n} \frac{d\tau'}{\mu_n} & (\mu_n > 0)\,, \end{cases} \quad (4)$$

where subscript n (≥ 1) denotes the nth order scattered light. The source density that gives rise to this intensity is

$$S_n(\tau', \mu_n) = \frac{a}{2} \int_{-1}^{1} I_{n-1}(\tau', \mu_{n-1}) \phi(\mu_n, \mu_{n-1})\, d\mu_{n-1} \quad (n \geq 1)\,, \quad (5)$$

where a (~ 0.5) is the albedo and ϕ is the phase function, both taken from Mathis, Mezger, & Panagia (1983). The total intensity at any point (e.g., the point A in Fig. 1) in the dust disk toward any direction $\mu' = \cos(i')$ is then found from

$$I(\tau_1, \mu') = \sum_{n=0}^{\infty} I_n(\tau_1, \mu')\,. \quad (6)$$

As pointed out by van de Hulst & de Jong (1969), for small τ and $a \leq 1$ this series converges rapidly. In practice we took the first 20 terms in the summation. For the adopted albedo and phase function, this gives an approximation to equation (6) with an accuracy of 10^{-5} for $\tau \leq 10$.

Using the radiative transfer model, we then calculate the ratio between the light absorbed by dust (dust heating) at a certain frequency λ and the light escaped and eventually observed at the same frequency, as a function of the optical depth of the disk at that frequency, τ_λ, and the view angle:

$$G(\tau_\lambda, \mu) = \frac{\int_0^{\tau_\lambda} [\int_{4\pi} I_\lambda(\tau_1, \mu')\, d\omega](1 - a)\, d\tau_1/\mu}{I_\lambda(0, \mu) + E_1/\mu}\,, \quad (7)$$

where $I_\lambda(0, \mu) + E_1/\mu$ is the prediction for the light observed, $\mu = \cos(i)$ (for M31, $i = 77°$), τ_λ is the optical depth of the disk (seen face on), ω is the solid angle, and a is the albedo. The factor $(1 - a)$ gives the ratio between the absorption cross section and the extinction cross section. It is worthwhile to note that the resulting value of $G(\tau, \mu)$ is not sensitive to the values of E_1 and E_2 as long as the disk is optically thin. It should be mentioned that, although not used in this work, the model also calculates the extinction:

$$A_\lambda = 2.5 \log \left[\frac{(E_1 + E_2 + S_0 \tau_\lambda)/\mu}{I_\lambda(0, \mu) + E_1/\mu} \right]. \quad (8)$$

We calculate dust heating caused by UV light (912 Å $< \lambda \leq$ 3000 Å) and that caused by optical and near-infrared (NIR) light (3000 Å $< \lambda \leq$ 9000 Å) separately and assume that dust heating caused by radiation of wavelength greater than 9000 Å is negligible. The stars most responsible for the nonionizing UV radiation (B stars) presumably have similar scale height as that of the dust (Mathis et al. 1983). Therefore, for the UV radiative transfer model we assume that both z_1 and z_2 in Figure 1 are equal to zero, and so the values of E_1 and E_2 in equation (1) are also equal to zero. On the other hand, it is likely that the older stars responsible for the optical radiation have larger scale height than the dust. We assume that stars which lie outside the dust layer radiate half the total optical radiation, and that $E_1 = E_2 = 0.5 \times S_0 \tau$.

The only UV photometry observations covering the whole M31 field have been made by the Marseille group (Deharveng et al. 1980; Milliard 1984) at 2030 Å. Therefore, we calculate the UV heating using the formula

$$I_{\rm fir}^{\rm UV} = I_{2030}\, 10^{0.4 A_{2030}^{G}}\, G(\tau_{2030}) \times \int_{912\ \text{Å}}^{3000\ \text{Å}} 10^{-0.4[m(\lambda)-m(2030\ \text{Å})]}\, \frac{G(\tau_\lambda)}{G(\tau_{2030})}\, d\lambda\ , \quad (9)$$

where $I_{\rm fir}^{\rm UV}$ is the FIR radiation intensity caused by UV heating; I_{2030} is the 2030 Å radiation intensity taken from the UV map (Milliard 1984), in units of ergs cm^{-2} s^{-1} Å^{-1} arcsec^{-2}; and τ_{2030} is the optical depth of the disk at 2030 Å. We have omitted the variable μ in the expression of $G(\tau_\lambda)$ because here $\mu = \cos(77°)$ is fixed. A_{2030}^{G} is the foreground Galactic extincton at 2030 Å. Burstein & Heiles (1984) found that in the direction of M31, the Galactic reddening is $E(B-V)_G = 0.8$ (see also van den Bergh 1991). According to Savage & Mathis (1979),

$$A_{2030}^{G} = 8.67 \times E(B-V)_G = 0.69\ \text{mag}\ . \quad (10)$$

The adopted UV spectrum $[m(\lambda) - m(2030\ \text{Å})]$ and selective UV extinctions (τ_λ/τ_v) are given in Table 1. Following Koper (1993), the UV spectrum is estimated from the mean of the UV spectra of 29 fields in the M31 disk, each 2.5 × 2.5 in size, observed by Israel, De Boer, & Bosma (1986) in five UV bands: 1550, 1800, 2200, 2500, and 3300 Å. It is likely that the UV spectrum changes from place to place in a spiral disk, which may introduce an error into our model calculation. However, this is only the second order compared to the uncertainties resulting from errors in the absolute flux at 2030 Å. In addition, since the UV heating is never dominant for the diffuse dust in the M31 disk (§ 4.2), this uncertainty will have little effect on our results. The UV extinction curve is taken from Hutchings et al. (1992), who found a much shallower and narrow 2175 Å bump compared to the Galactic extinction curve (Savage & Mathis 1979). The magnitude and the selective extincton at 912 Å are obtained from extrapolation of the available UV data reported in Table 1.

TABLE 1

UV Spectrum and Selective Extinction of M31

λ (Å)	$m_\lambda - m_{2030}$ (mag)	τ_λ/τ_v	Reference
1550.....	−0.33	3.47	1
1800.....	−0.15	3.06	1
2030.....	0.00	2.74	1
2200.....	0.08	2.82	1
2500.....	0.28	2.14	1
3000.....	0.48	1.75	1
3650.....	...	1.53	2
4400.....	...	1.35	2
5500.....	...	1.00	2
7000.....	...	0.82	3

References.—(1) Hutchings et al. 1992. (2) Walterbos & Kennicutt 1988. (3) Savage & Mathis 1979.

We have more information about the spectral distribution of the optical radiation field in M31. Digitized photographic surface photometry maps in three optical bands (Walterbos & Kennicutt 1987), namely, the U band ($\lambda_1 = 3650$ Å), B band ($\lambda_2 = 4400$ Å), and V band ($\lambda_3 = 5500$ Å), are available to us. The R band ($\lambda_4 = 7000$ Å) magnitude of each pixel in the M31 field can be estimated from the V magnitude using the average $(V-R)$ color of M31 (WK88):

$$V - R = 0.72\ , \quad (11)$$

which is rather constant in the disk of M31 without any significant gradient along the galactocentric radius (WK88).

Thus we can calculate the dust heating by the radiation at the four corresponding wavelengths:

$$I_{\rm fir}^{\rm op,\,1} = I_i \times 10^{0.4 A_i G}\, G[\tau(\lambda_i)]\ , \quad (12)$$

where $i = 1$, 2, 3, and 4 correspond to U, B, V, and R bands, respectively. Three of four optical selective extinctions $[\tau(\lambda_i)/\tau_v, i = 1, 2, 3]$ are taken from WK88, while selective extinction τ_R/τ_v is taken from the local value (Savage & Mathis 1979). They are also listed in Table 1. The other two points, $I_{\rm fir}^{\rm op,\,0}$ and $I_{\rm fir}^{\rm op,\,5}$ are extrapolated to $\lambda_0 = 3000$ Å and $\lambda_5 = 9000$ Å from the four points described above. The final estimate of the optical heating of the diffuse dust is calculated from

$$I_{\rm fir}^{\rm op} = \sum_{i=0}^{5} 0.5(I_{\rm fir}^{{\rm op},i} + I_{\rm fir}^{{\rm op},i+1})(\lambda_{i+1} - \lambda_i)\ . \quad (13)$$

The sum of the optical heating and UV heating,

$$I_{\rm fir}^{\rm tot} = I_{\rm fir}^{\rm op} + I_{\rm fir}^{\rm UV}\ , \quad (14)$$

estimates the total heating. In order to compare it with the FIR surface brightness $I_{\rm fir}$, we have to estimate the fraction of dust reradiation in the wavelength range of 40–120 μm. Fitting the mean *IRAS* colors of M31 cirrus (Xu & Helou 1994) with a grain model assuming that the very small grains are only half as abundant in M31 dust as they are in Galactic cirrus (Xu & Helou 1994), we find

$$f = \frac{I(40\text{–}120\ \mu\text{m})}{I(8\text{–}1000\ \mu\text{m})} = 0.32 \pm 0.06\ . \quad (15)$$

The 1 σ error is estimated from the uncertainties of the mean *IRAS* colors and does not include the uncertainties of the model. In particular, in cases in which the FIR emission is dominated by very cold grains ($T \sim 10$ K) which emit almost all their energy outside *IRAS* bands, the expression in equation (15) may overestimate the fraction. On the other hand, given the very sensitive dependence of dust emission on temperature (§ 1), very cold grains can rarely dominate the dust emission. For grains warmer than 15 K (ν^2 emissivity law), expression (15) is accurate within 40%.

In the model of dust heating and cooling, the only free parameter is τ_v, the optical depth at 5500 Å. The following equation, which balances the cooling rate (the FIR emission) to the heating rate, determines τ_v:

$$I_{\rm fir} = I_{\rm fir}^{\rm tot}(\tau_v) f\ , \quad (16)$$

where $I_{\rm fir}$ is the observed FIR (40–120 μm) surface brightness.

4. RESULTS

4.1. *Optical Depth and Optical Depth–to–Gas Ratio*

A gray-scale plot of the distribution of the V-band optical depth seen from 77° inclination angle, τ_v, calculated using the above model for the cells selected, is presented in Figure 2. The range of the gray scale is between $\log(\tau_v) = -0.4 (\tau_v = 0.4)$ and $\log(\tau_v) = 0.6$ ($\tau_v = 4$). Because of the selection criteria of the cells (see § 2), not all of the disk of M31 is covered in this plot; in particular, the star formation regions as indicated by discrete FIR sources have been deliberately left out. There are several spots in which the dark cells ($\tau_v \gtrsim 2$) are concentrated, most of them in the "ring." There is a general trend that in the inner disk the optical depth tends to be relatively low, and in the ring the optical depth tends to be high.

In Figure 3 we plot τ_v versus the galactocentric radius for the same sample of M31 cells. The large filled squares with error bars are the means and dispersions for cells in different radius bins, each spanning 2 kpc. The optical depth increases with radius from $\tau_v \sim 0.7$ at $r = 2$ kpc in the inner part of the disk, reaching a peak of $\tau_v \sim 1.6$ at about 10 kpc, and staying quite flat out to 14 kpc. Beyond 14 kpc, no cells are detected in FIR above the 5 σ threshold. This 5 σ threshold might bias the mean values of the optical depth toward higher values, in particular for the innermost and outermost bins where the low FIR emission regions are most likely to be found, because the low FIR surface brightness cells generally have low τ_v. In order to check this possibility, we have calculated the means of τ_v for the same bins using another sample including all cells with signal-to-noise ratio of the FIR surface brightness above a factor of 2. No significant difference is found compared to the means plotted in Figure 3, although the dispersions are increased because of the larger errors in the data. Hence, the bias mentioned above is not significant. For cells in the immediate vicinity of massive star formation regions, there is another source of uncertainty, namely, that the dust heating model (§ 3) ignores heating by ionizing radiation. This results in an overestimate of the optical depth for the cells. However, because the sample were selected against such cells which in any case occupy only a small part of the M31 disk, this error shall not affect the means significantly.

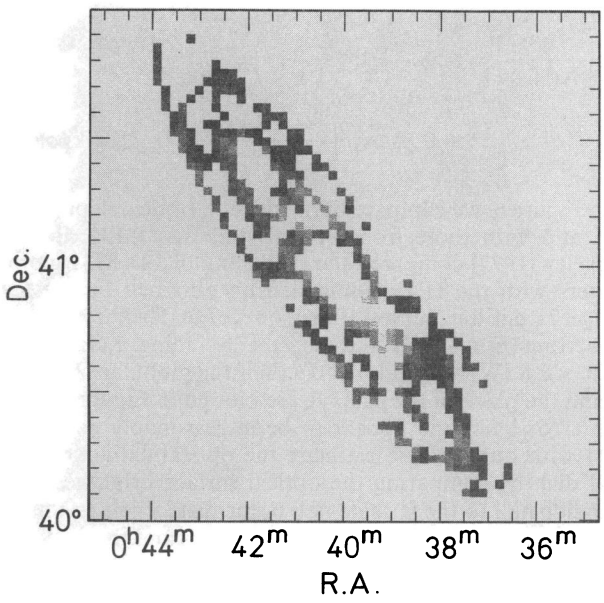

FIG. 2.—Gray-scale plot of τ_v, the V-band (5500 Å) optical depth viewed from the inclination angle $i = 77°$, in the M31 disk. Areas containing considerable contribution from discrete sources ($I_{60\mu m,s}/I_{60\mu m} > 0.2$) are not included. The range of the gray scale is between $\log(\tau_v) = -0.4$ (the faintest) and $\log(\tau_v) = 0.6$ (the darkest), and the intermediate gray levels correspond linearly to the $\log(\tau_v)$ levels.

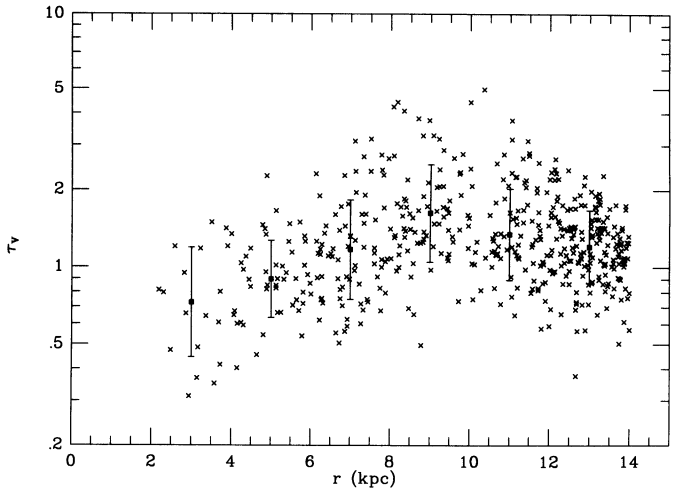

FIG. 3.—Radial distribution of τ_v. Crosses are results for M31 cells (size of 2′ × 2′). Filled squares with error bars are means for cells in six bins, each spanning 2 kpc in the plane of M31. Error bars give the 1 σ dispersions.

It should be noted that the overall distribution of τ_v is rather flat, which disagrees with a popular assumption (Disney, Davies, & Phillipps 1989; Byun, Freeman, & Kylafis 1994) that the optical depth and stars have the same central-peaked exponential r-distribution in spiral disks. Another point we want to make is that the face-on optical depth in the disk of M31 should be a factor of 4.4 lower than τ_v, which is seen from 77° inclination angle. The results presented in Figure 3 then indicate that in the M31 disk the face-on optical depth is in the range of 0.2–0.4, namely, that the disk is optically thin, inconsistent with the hypothesis that spiral disks are "opaque" (Valentijn 1990).

In Figure 4 we compare our results, for which the error bars now represent the statistical uncertainty of the means [uncertainty = dispersion/$(N-1)^{1/2}$], with the distributions of the neutral atomic gas (Brinks & Shane 1984) and of the molecular hydrogen gas estimated by Koper et al. (1991) from the CO observations, and that of the dust clouds (Hodge 1980). It appears that the τ_v distribution shows a similar r-dependence as the H I gas distribution, while the molecular gas distribution is very different, characterized by two very narrow peaks at $r \sim 4$ kpc and at ~ 10 kpc, respectively. This result suggests a correlation between column densities of the H I gas and the diffuse dust. However, the τ_v versus H_2 comparison must be made with caution. First of all, regions in which the molecular gas is concentrated are underrepresented in the sample of cells owing to the exclusion of cells dominated by discrete sources (active star formation regions). And second, there seems to be large uncertainties with the H_2 map deduced from the CO survey of Koper et al. (1991), in particular in the inner part of the disk. Allen & Lequeux (1993; see also Allen et al. 1994) detected very cold (close to the 2.7 K cosmic background temperature) CO emission in two dust clouds in the inner region of M31 ($r \lesssim 2$–3 kpc) which may contain as much as a

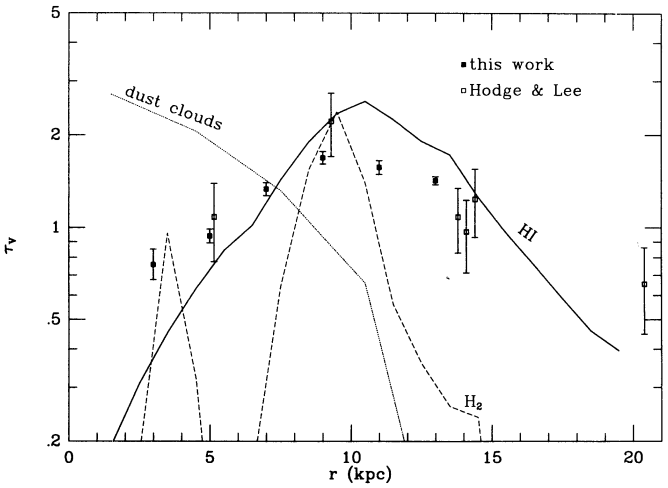

FIG. 4.—Comparison of the radial distribution of optical depth τ_v with the radial distributions of the H I (Brinks 1984), of the H_2 gas estimated from CO (Koper et al. 1991), and of dust clouds (Hodge 1980). The column densities of gas and the column density of dust clouds are in arbitrary units. Also plotted are the results of the star-reddening study by Hodge & Lee (1988). The mean optical depths of six radial bins are given by the filled squares, with the error bars representing the statistical uncertainty [= dispersion/$(N-1)^{1/2}$].

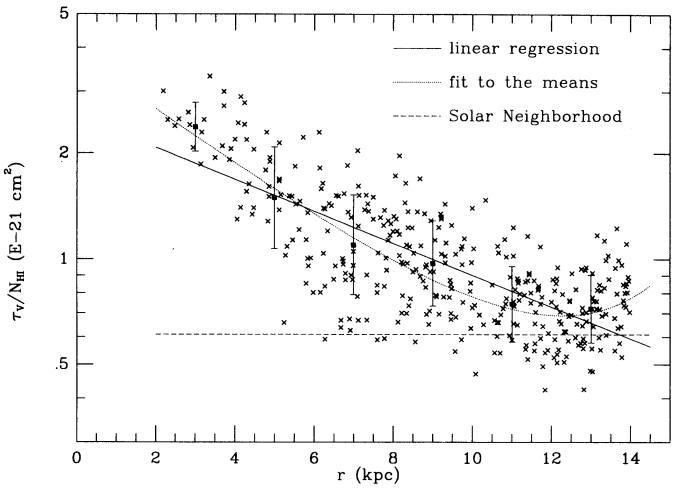

FIG. 5.—Radial distribution of the optical depth to H I column density ratio τ_v/N(H I). Crosses are results for M31 cells. Filled squares with error bars are means for cells in six bins, each spanning 2 kpc in the plane of M31. The error bars give the 1 σ dispersions. The solid line represents the linear regression calculated for the sample of cells (358 of them). The dotted curve is a smooth fit to the means, given by equation (18) in the text. The dashed horizontal line indicates the τ_v–to–H I gas ratio in the solar neighborhood taken from Savage & Mathis (1979).

few times $10^7\ M_\odot$ molecular gas and may have a CO to H_2 conversion factor of about 1 order of magnitude higher than the average value taken by Koper et atl. (1991). The surface density of dust clouds decreases rapidly and monotonically with increasing radius, perhaps as a result of the selection effect that clouds close to the center of the galaxy are easily detected on an optical image (Hodge 1980) because of the high brightness of the disk.

We also plotted the results of Hodge & Lee (1988), denoted by the open squares with error bars, from a reddening study for stars (most in OB associations) in six M31 fields with different galactocentric radii. Assuming that the stars are located in the middle of the dust layer, the reddening [E($B-V$)] reported in that paper has been converted to τ_v by multiplying a factor of $2 \times 0.921 \times 2.8$ (WK88). In spite of the fact that completely different approaches are used, a good general agreement is found between the results of Hodge & Lee (1988) and ours, with the former being only slightly higher where the two data sets overlap. The difference may result from their fields being biased for star formation regions, while ours are biased against such regions.

In Figure 5 we plot for the sample of M31 cells the optical depth–to–H I gas ratio versus the galactocentric radius. The dashed line represents the optical depth–to–H I gas ratio in the solar neighborhood (Savage & Mathis 1979). It appears that the ratio in M31 is in general slightly higher than that in the solar neighborhood. A clear trend of decrease of the ratio with increasing radius is evident. The linear regression of the plot gives

$$\log\left[\frac{\tau_v}{N(\text{H I})}\right] = 0.41(\pm 0.02) - 0.045(\pm 0.002)\left(\frac{r}{1\ \text{kpc}}\right), \quad (17)$$

where N(H I) is in units of 10^{21} atoms cm^{-2}. The slope (-0.045 ± 0.002) corresponds to an e-folding scale length of 9.6 ± 0.4 kpc for the galactocentric gradient of the optical depth–to–H I gas ratio in M31. It is interesting to note that our optical depth–to–H I gas ratio gradient is consistent with the metallicity gradient found by Blair, Kirshner, & Chevalier (1982), which ranges from 9.8 kpc (for the N/H abundance ratio) to 14.9 kpc (for the O/H abundance ratio). The solid squares with error bars in Figure 5 are the mean ratios of cells in different radius bins, each 2 kpc wide. The error bars represent 1 σ dispersions and amount only to about 30%. The dotted curve is a smooth fit to the means which can be expressed as

$$\log\left(\frac{\tau_v}{N(\text{H I})}\right) = 0.58 - 0.08\left(\frac{r}{1\ \text{kpc}}\right) + 0.22\exp\left(\frac{r-12\ \text{kpc}}{3\ \text{kpc}}\right) \quad (r \le 14\ \text{kpc}). \quad (18)$$

In Figure 6, we compare our results on optical depth–to–H I gas ratio with those from optical studies of M31. Bajaja & Gergeley (1977) compared the reddening of 121 M31 globular clusters with the H I column density obtained by the Cambridge 21 cm line survey (Emerson 1974). Their results, after converting $E(B-V)$/H I to τ_v/H I assuming $\tau_v/E(B-V) = 0.921 \times 2.8$ (WK88) and $p = 0.5$ (half the globular clusters are behind the plane of the galaxy), are plotted in Figure 6 (crosses with error bars) and appear to be in reasonably good agreement with ours. WK88 estimate the optical extinction in the M31 disk by comparing the optical surface brightness of the near-side half to the far-side half of the disk. Their results, also plotted in Figure 6, fall below our estimates and those of Bajaja & Gergeley (1977) possibly because, as suggested by WK88, they are only lower limits of true values. It should be noted that the real difference between our results and those of WK88 could be even larger because in their calculation of τ_v/H I they have used the "disk H I" map of M31 (Brinks & Burton 1984), derived from the total H I map (Brinks & Shane 1984) under the assumption that the H I disk of M31 is warped (Brinks &

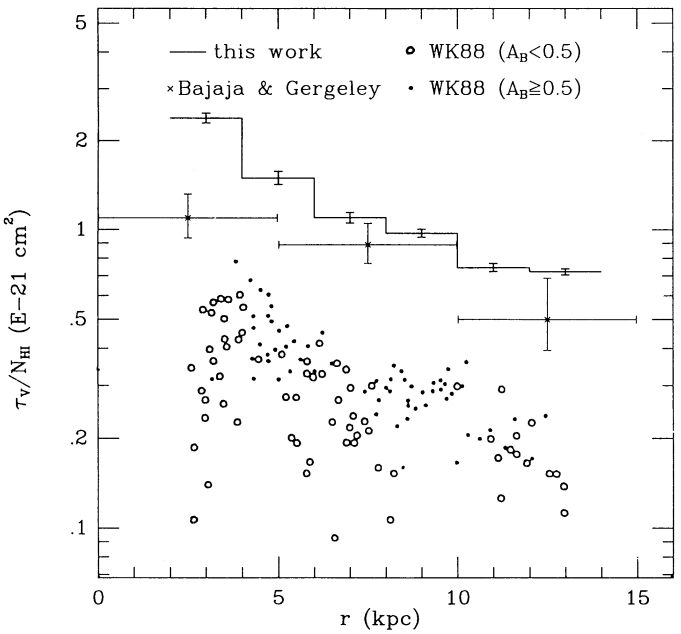

FIG. 6.—Comparison of the radial distribution of the τ_v-to-H I gas ratio obtained in this work with the results of Bajaja & Gergeley (1977) and those of Walterbos & Kennicutt (1988, WK88).

Burton 1984). The "warp model" has been questioned by Braun (1991) who proposed alternatively a "sticking out arm segments" model to interpret the different H I velocity components. We have used in this study the map of the total H I column density without the disk/warp decomposition.

We introduce a gradient-corrected optical depth:

$$\tau_{v,c} = \tau_v \exp\left(\frac{r}{9.6\ \mathrm{kpc} - 1}\right), \qquad (19)$$

which we plot against H I column density in Figure 7, with

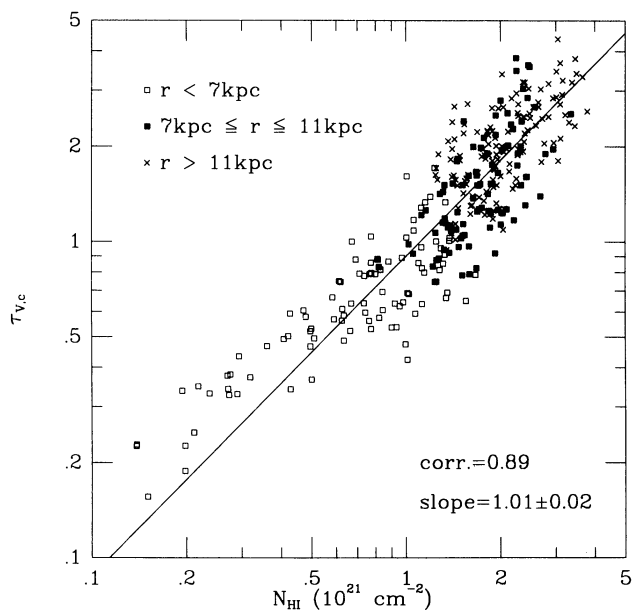

FIG. 7.—Plot of the "gradient-corrected" optical depth vs. H I column density. Cells in different parts of the disk are denoted by different symbols. The solid line represents the linear regression of the data.

different symbols denoting cells in the inner disk ($r < 7$ kpc), in the "ring" ($7 \leq r \leq 11$ kpc), and in the outer disk ($r < 7$ kpc). A strong and linear correlation is found in this log-log plot: the correlation coefficient is 0.89. The dispersion of the logarithm of $\tau_{v,c}/N$(H I) ratio is 0.12, i.e., 32% on a linear scale. The slope of the least-squares fit shown by the solid line is 1.01 ± 0.02. These results suggest that for a given galactocentric radius the dust column density, as indicated by τ_v, scales closely and linearly with the column density of H I gas, while the scaling factor decreases with increasing galactocentric radius, reflecting the gradient in the dust–to–H I gas ratio. Tight local correlation between dust and H I gas has been detected in the solar neighborhood (Savage & Mathis 1979; Boulanger & Pérault 1988).

It should be noted that taking into account the molecular gas component may affect the estimated gradient of the optical depth–to–gas ratio expressed in equation (17). In particular, the high mean ratios in the first two bins in Figure 5 might indeed be caused by the large amount of very cold molecular gas hiding in the inner part of the M31 disk, suggested by the observations of Allen & Lequeux (1993). And some of the scatter in Figure 5 may also result from the neglect of the molecular gas. On the other hand, we would recall that (1) globally speaking it is likely that the H I phase contains the bulk of interstellar gas in the M31 disk (Koper et al. 1991); (2) a large percentage of the dust associated with molecular gas should concentrate in star formation regions (Cox & Mezger 1989), and its contribution could therefore have been greatly reduced, though not completely removed, by our removal of discrete sources.

4.2. *Total Dust Mass and Global Dust-to-Gas Ratio*

In order to convert τ_v to dust column density, we assume that in the M31 disk the ratio of τ_v to dust column density is the same as that in the solar neighborhood (Désert et al 1990), namely, that dust in M31 has the same opacity as dust in the solar neighborhood. This is plausible because in the M31 disk the composition and size distribution of the large normal grains which dominate the dust mass (Draine & Lee 1984) may be similar to those in the solar neighborhood, given that the optical extinction is mainly caused by large grains and that the optical extinction curve of M31 is similar to that in the solar neighborhood (WK88). Thus, using the H I map (Brinks & Shane 1984) and the mean τ_v–to–H I gas ratios for different radial bins, we estimate that there is $1.9 \times 10^7\ M_\odot$ dust, with an error in the order of 30% including the uncertainties resulting from the data and from the model calculation, within the M31 disk between $r = 2$ kpc and $r = 14$ kpc.

Within the same radius range we estimate that, using the H I data of Brinks & Shane (1984), there is $1.8 \times 10^9\ M_\odot$ H I gas and, according to Koper et al. (1991), $2.5 \times 10^8\ M_\odot$ "warm" H_2 gas. The amount of very cold H_2 such as found by Allen & Lequeux (1993) in the inner disk is not known. If this component is confined to galactocentric radii less than ~3–4 kpc with a surface density $\sim 3\ M_\odot\ \mathrm{pc}^{-2}$ (Allen & Lequeux 1993), a rough estimate yields a mass of $\sim 10^8\ M_\odot$. Therefore, in the M31 disk the global dust-to-gas ratio is $9.0(\pm 2.7) \times 10^{-3}$, indeed very close to the solar neighborhood value of 7.3×10^{-3} (Desert et al. 1990).

4.3. *Energy Budget of the Diffuse FIR Emission*

In our model it is assumed that the diffuse interstellar dust is heated by ISRF in the nonionizing UV (912–3000 Å) and

optical–near-infrared (NIR) (3000–9000 Å) bands. In principle, different stellar populations can be held responsible for the ISRF in these bands: the UV radiation comes mainly from B stars (4–20 $M_\odot$) which live only $\lesssim 10^8$ yr, and the optical-NIR radiation comes from less massive, older stars ($\gtrsim 10^9$ yr). In this sense, the question of which stellar population is most responsible for the heating of the diffuse dust in M31 can be investigated by estimating the relative contributions of the radiation in these different bands to the dust heating.

We apply the dust heating model (§ 3) to a set of galactocentric annuli, each of 6′ width (1.2 kpc) in the M31 plane, covering from 2 kpc to 14 kpc. The average optical depth of each annulis is estimated from the average H I column density, assuming the radius dependence of the optical depth–to–H I gas ratio as specified by equation (18). In Figure 8 the solid line is the radial distribution of the FIR surface brightness, and the dashed line is the diffuse FIR emission predicted by the heating model. The significant difference between them around the ring and in the outer region of the disk comes from the discrete sources, most of which are in these parts of the disk (Fig. 3 in Paper I). Otherwise, the difference is less than 10%, well within the uncertainty of the heating model. This is expected because the optical depth–to–H I gas ratio adopted here is estimated from the FIR versus heating comparison for the diffuse dust (§ 4.1). The nonionizing UV radiation contributes only 27% of the total heating, represented by the dot-dashed curve in Figure 8. It is most prominent at the ring, but never dominant. Throughout the M31 disk, the optical radiation, shown as the dotted curve, dominates the heating of the diffuse dust. This indicates that the diffuse FIR emission of M31 is mainly caused by heating by the optical radiation from relatively old stars, i.e., stars older than a few $\times 10^9$ yr. Xu (1990) found that on average the nonionizing UV radiation contributes 56%–76% of heating of diffuse dust in spiral galaxies. The UV heating of diffuse dust in the M31 disk appears to be much less significant than for a more typical spiral galaxy (e.g., the Milky Way). This is because of the very low 2000 Å–to–blue flux ratio of M31, actually one of the lowest in a large sample of nearby galaxies (Buat & Xu 1995), a consequence of the very low recent star formation rate of M31.

5. DISCUSSION

5.1. *Uncertainties Introduced by Assumptions in the Model*

As discussed in § 3, our model for dust heating and cooling is insensitive to the assumptions on the physical conditions of dust (e.g., thermal equilibrium and T_d) and to the grain model which is still poorly known (Désert et al. 1990). The only parameter affected by these factors is f in equation (16), which estimates the fraction of dust emission in the wavelength range 40–120 μm. Since our result on optical depth depends on f at most linearly, whereas in optically thick cases only logarithmically, we argue that the uncertainty introduced through f cannot be very large. On the other hand, there are some other uncertainties as a result of various assumptions made in our model, all for the sake of simplicity, which we discuss in this section.

We have assumed implicitly in the model that each cell (0.4 × 1.8 kpc^2) is independent of the others, which is strictly not true; stars in neighboring cells can contribute significantly to the heating of dust in a given cell, since the photon mean

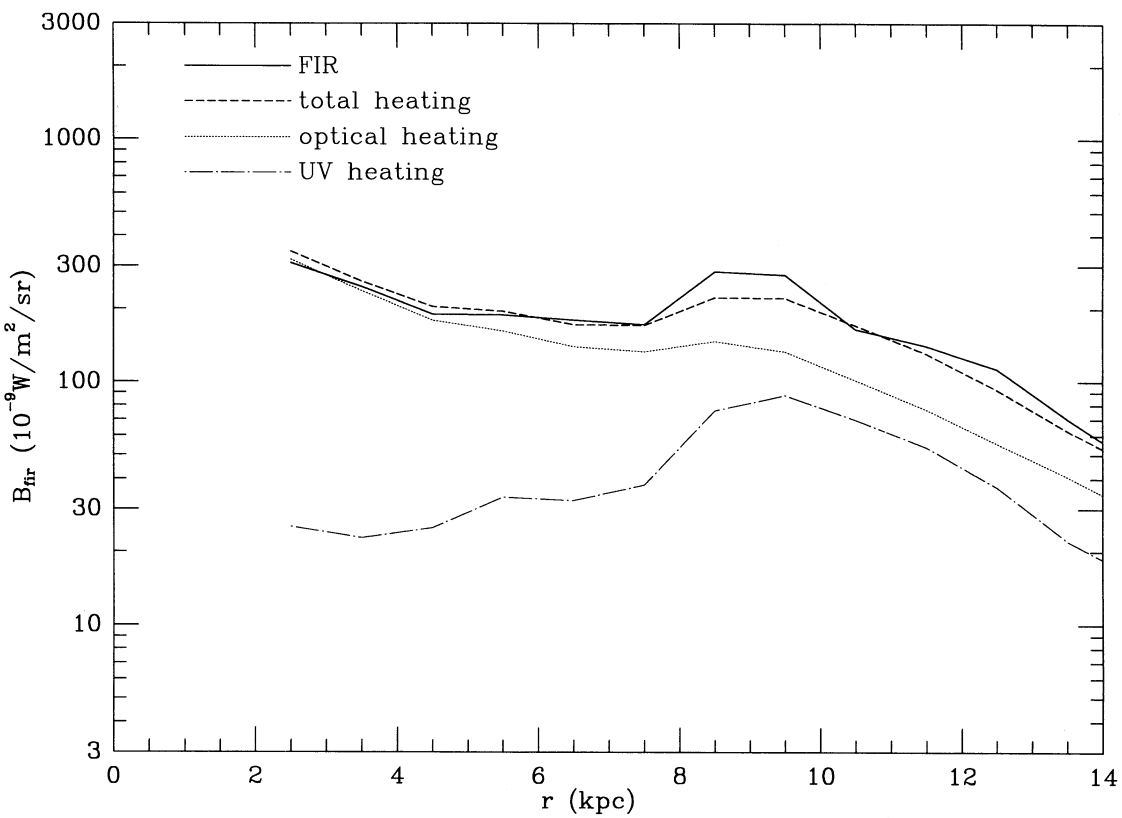

FIG. 8.—Radial distribution of the contribution to the FIR emission from the heating of diffuse dust by the UV (912–3000 Å) radiation and by the optical (3000–9000 Å) radiation. Also plotted are the sum of the two contributions ("total heating"), and the observed FIR surface brightness distribution.

free path is usually larger than the size of the cells. This is a reasonable assumption, however, as long as the physical conditions do not change abruptly between adjacent cells, and it is likely to hold in most cases at least for the optical emission which dominates the dust heating (§ 4.3), given the rather smooth distribution of the optical surface brightness (Walterbos & Kennicutt 1987).

How reliable is the homogeneity assumption for the dust distribution? Hodge (1980) cataloged dust clouds of different sizes throughout the M31 disk, and Allen & Lequeux (1993; see also Allen et al. 1994) reported very cold and dense molecular clouds associated with two of these dust clouds (D268 and D487) in the inner disk. If the interstellar dust is concentrated in these dust clouds, and if the clouds are highly optically thick, then the radiative transfer problem in the M31 disk can be very different from our model of a uniformly distributed dust plane. Hodge & Kennicutt (1982) found that M31 dust clouds are in general optically thin. This is confirmed by the recent study of Sofue & Yoshida (1993), who studied the reddening of a complex of M31 dark clouds, including D382, D384, and D395 in Hodge's catalog. The peak reddening is only $E(B-V) \simeq 0.2$, corresponding to $A_v \sim 0.6$ mag. Allen et al. (1994) estimated that the clouds they studied for very cold molecular gas causes a moderate extinction ($A_v = 2 \pm 1$ mag). As demonstrated in the studies of Boissé (1990) and Hobson & Scheuer (1993) (see also Caplan & Deharveng 1986), clumpy media with the same amount of dust will always cause less extinction with a flatter extinction curve than homogeneous media do. The optical extinction law in M31 found by WK88 (see also Hodge & Kennicutt 1982) is not very different from that of the diffuse dust in the solar neighborhood (but also see Iye & Richter 1985). Therefore, we conclude that most of the diffuse dust not associated with star-forming regions in the M31 disk is optically thin, and our analysis is affected only to second order by inhomogeneities. However, it should be noted, as pointed out by Allen et al. (1994), that the dust clouds themselves may be very clumpy, containing very high density regions ($A_v \sim 10$ mag) with very small filling factors. Dust associated with these tiny dark clumps will be largely missed by our model. While the possibility of missing the coldest dust adds to the uncertainty of the τ_v profile we derive, it has less of an impact on the estimated dust-to-gas ratio, precisely because the estimation of τ_v attaches greater weight to the H I component of the interstellar medium.

Another uncertainty may be the result from the variation of the relative location of the dust layer and the stellar disk. In our model, we adopted a "sandwich" configuration in which the dust layer is in the middle of the stellar disk. In a dynamical analysis, Braun (1991) found that several arm segments of H I gas stick out of the disk as far as ~ 1 kpc. If the dust is mixed with H I in these arm segments, they should be foreground or background relative to the stars. If these arms are optically thin, the uncertainty caused by this on our dust heating model is not very significant, because the G ratio in equation (7) is then approximately proportional to the optical depth regardless of the location of the dust layer. On the other hand, if they are very optically thick, this can cause a dramatic effect because the UV and optical radiation can be totally extinguished when the layer is foreground, or extinction free when the dust layer is background. The disk of M31, viewed at 77° inclination angle, is marginally optically thick ($\tau_v \sim 1$, see § 4.1). Therefore, we checked for evidence of such geometric effect.

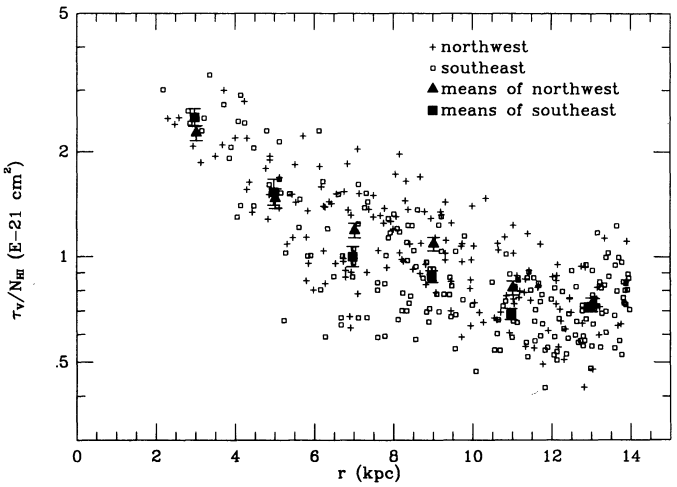

FIG. 9.—Comparison of radial distributions of τ_v-to-$N_{H\,I}$ ratio of cells in the northwest half (near half) and in the southeast half (far half). The error bars of the means represent the statistical uncertainties of the means.

In Figure 9 we plot the optical depth–to–H I ratios of M31 cells in the northwest half (near half) and in the southeast half (far half) with different symbols as described in the legend. The large filled and open squares with error bars (statistical uncertainties) are means of cells in different radius bins (2 kpc in width), for the northwest half (near half) and the southeast half (far half), respectively. There is a systematic difference between the dust–to–H I ratios of the two halves in the sense that the cells in the near half tend to have higher ratios and those in the far half have lower ratios. This difference is statistically significant (at $\sim 3\,\sigma$ level) in the three bins $6 \leq r \leq 8$ kpc, $8 \leq r < 10$ kpc, and $10 \leq r < 12$ kpc, where the "ring" is encompassed, although the absolute values of the difference are never very large (at $\sim 20\%$ level). This difference might reflect real changes of the dust properties in the two halves. However, it may also be artificial if the "sandwich" configuration assumed in our model is violated. Running a model which is otherwise the same as that in § 3 except that the position of the dust layer is adjustable, we found that the near half/far half difference can be accounted for if, in the galactocentric radius range encompassing the "ring" (7 kpc $< r <$ 12 kpc), the dust layer in the near half is displaced with respect to the stellar disk toward us by a distance of half its thickness, or the dust layer in the far half is displaced away from us by about the same distance, or the dust layers in both halves are displaced by a distance of one-third of their thickness toward and away from us, respectively. Interestingly, these possible deviations of the dust layer from the middle plane in the two halves of M31 are consistent qualitatively with the H I warp reported by Braun (1991). No significant differences on the galactocentric gradient of the optical depth–to–H I gas ratio and on the total dust content of M31 are introduced by these possible displacements.

5.2. *FIR versus UV-optical Comparison as a Tool for Studying Extinction and Dust-to-Gas Ratio in Galaxies*

The dust heating and cooling model presented in this paper can be used to address the widely debated problem about the extinction in disk galaxies (Disney et al. 1989; Valentijn 1990). Except for a few Local Group galaxies, including the Magellanic Clouds (Koornneef 1982; Fitzpatrick 1986), M31 (Hodge &

Lee 1988; Bajaja & Gergeley 1977), and M33 (Humphreys, Bowyer, & Martin 1990; Bianchi, Hutchings, & Massey 1991), in which individual stars or star clusters can be resolved, direct reddening/extinction studies through optical observations are not possible for galaxies in general. Indirect methods such as the statistical analysis of the inclination dependence of the surface brightness and the isotophal diameter lead to controversial results (Holmberg 1958; Valentijn 1990; Burstein, Haynes, & Faber 1991), possibly because of various selection effects (Disney 1992). Block et al. (1994) proposed that optical minus NIR colors ($B-K$ and $V-K$) can be used as extinction indicators. But the quantitative result of the method depends sensitively on the assumed intrinsic colors which change with the stellar population. In principle, the extinction can be estimated from the dust column density for which the FIR and submillimeter surface brightness might be used as an indicator. However, because of the sensitive dependence of the dust emission model on the temperature and on the poorly known FIR emissivity law of grains, the column density of dust, and therefore the optical depth, estimated from the emission of dust grains alone is very uncertain (Kwan & Xie 1992; Chini & Krügel 1993).

In our model, the FIR/UV-optical ratio has been used as an extinction indicator, under the reasonable assumption that all the radiation absorbed by dust in UV and optical will be reradiated in the infrared. Quantitative results are obtained using a radiative transfer model (§ 3). Good agreements with optical studies of extinction in M31 (Hodge & Lee 1988; Bajaja & Gergeley 1977; WK88) are found. Such a model can be easily extended to other disk galaxies for which the FIR, UV, and optical data are available. Indeed, Xu & Buat (1995) made such a study for a sample of 135 nearby spiral galaxies and found that most of spirals in their sample are optically thin to blue radiation ($\tau_B < 1$).

The results shown in § 4 also demonstrate that our model can be used to analyze quantitatively the dust-to-gas ratio in galaxies. The dust-to-gas ratios estimated using FIR and submillimeter emission of dust (Devereux & Young 1990; Rowan-Robinson 1992; Franceschini & Andreani 1995) are usually significantly lower than that found in the solar neighborhood, probably because of missing cold ($\lesssim 15$ K) dust (Block et al. 1994). Using our model, one estimates the dust column density from the extinction rather than from the emission. Since the extinction, unlike the emissivity, does not depend on grain temperature, our method in principle (particularly when submillimeter data are also available) can detect all dust grains no matter how cold they are, unless they hide in clumps of very high optical depth (Boissé 1990). This is illustrated in Figure 10, in which we plot for our sample of M31 cells the diagram of dust–to–H I gas ratio estimated using our model versus the dust–to–H I gas ratio estimated from the FIR emission by assuming that (1) the grains are in thermal equlibrium and (2) the temperature of grains are specified by the 60 μm to 100 μm flux ratio (ν^2 emissivity law). Both ratios are normalized by the value in the solar neighborhood. Although there is a good correlation in the plot, the dust-to-gas ratio estimated from the emission [$M_{d,100}/M$(H I)] is always significantly lower than that estimated from our model [$M_{d,v}/M$(H I)]. In particular, in the outer part of the disk where the intensity of the ISRF is low, and conseqently the FIR surface brightness is also low, the infrared-radiating dust accounts for only a few percent of the dust estimated from our dust heating/cooling model.

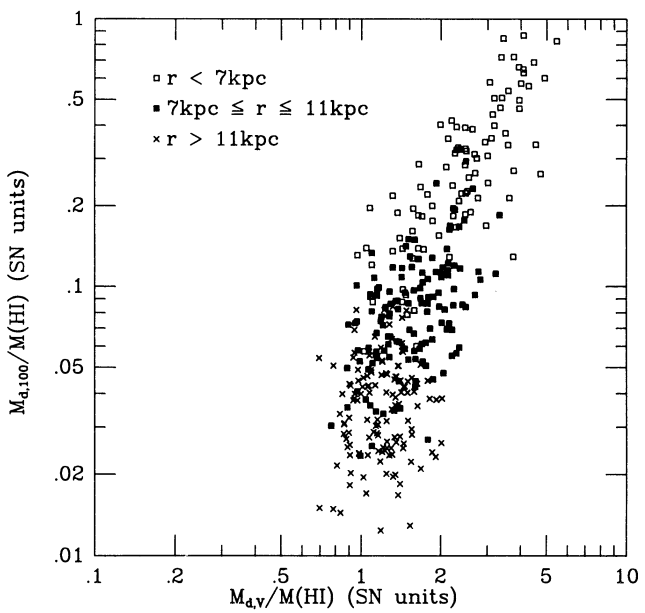

FIG. 10.—Comparison of the dust–to–H I gas mass ratio estimated using our model [$M_{d,v}/M$(H I)] and that estimated from the FIR emission [$M_{d,100}/M$(H I)]. Both are normalized by the value in the solar neighborhood. Cells in different parts of the M31 disk are denoted by different symbols.

6. SUMMARY

We have investigated the large-scale dust heating and cooling in the diffuse medium of M31 using far-infrared maps from *IRAS* in conjunction with the UV 2000 Å map by Milliard (1984), *UBV* maps by Walterbos & Kennicutt (1987), and the H I map by Brinks (1984). We analyse the areas of the M31 disk in which discrete sources contribute $\leq 20\%$ of the local 60 μm surface brightness, combining the cooling brightness (far-infrared) with the emerging portion of the heating brightness (912 Å $\leq \lambda \leq$ 9000 Å) to derive a mean optical depth τ_v for each cell ($\sim 0.4 \times 1.8$ kpc^2) in the M31 disk. This derivation is based on a plane-parallel radiative transfer model allowing for different thicknesses of the star layer and dust layer ("sandwich" model), which estimates heating input in each of 12 wavelength intervals, and accounts adequately for both absorption and scattering of light by dust. We find the following:

1. The mean optical depth (viewed from the inclination angle of 77°) increases with radius from $\tau_v \sim 0.7$ at $r = 2$ kpc outward, reaches a peak of $\tau_v \sim 1.6$ near 10 kpc, and stays quite flat out to 14 kpc, where the signal falls below the 5 σ level. Our results are consistent with earlier studies on stellar reddening and improve on them in spatial coverage and accuracy.

2. Compared to the radial profile of the H I gas and that of the molecular gas, the optical depth distribution resembles the former but differs significantly from the latter. This suggests a correlation between the H I gas and dust. However, the dissimilarity between the distributions of H_2 gas and of optical depth probably stems from the large uncertainty of the CO-to-H_2 conversion factor, and from the fact that H_2-rich regions are underrepresented in the sample of cells of *diffuse* regions.

3. The τ_v/N(H I) ratio decreases with increasing radius in the disk of M31, with an exponential law fit yielding an *e*-folding scale length of 9.6 ± 0.4 kpc. On average, the τ_v/N(H I) ratio in

M31 is not very different from its value in the solar neighborhood.

4. The optical depth adjusted for that radial gradient, i.e., $\tau_{v,c} = \tau_v[\exp(r/9.6\ \mathrm{kpc}) - 1]$ is strongly and linearly correlated with N(H I) over 1.5 orders of magnitude of column density. This indicates that at a given radius r the dust column density is proportional to the H I gas column density, with the proportionality factor decreasing with increasing r.

5. The portion of the M31 disk at radii between 2 and 14 kpc contains $1.8 \times 10^9\ M_\odot$ of H I gas and $2.5 \times 10^8\ M_\odot$ of H_2. Using the means of τ_v/N(H I) ratio at different galactocentric radii in the M31 disk and the dust opacity in the solar neighborhood, we derive from the H I map a corresponding total dust mass of $1.9 \pm 0.6 \times 10^7\ M_\odot$, yielding a global dust–to–total gas mass ratio of $9.0 \pm 2.7 \times 10^{-3}$. This value is about an order of magnitude larger than estimates based on emissivities and temperatures derived from 60-to-100 μm color ratios. We consider these smaller estimates less reliable because they are severely affected by the inadequacy of the single temperature assumption.

6. The nonionizing UV radiation, mainly coming from B stars (4–20 $M_\odot$), contributes only 27% of the heating of the diffuse dust in M31. This contribution is never locally dominant but is most prominent at the ring defined by H II regions and molecular clouds maxima. Throughout the M31 disk, heating of the diffuse dust is dominated by optical radiation from stars at least a billion years old.

We are very grateful to E. Brinks for providing the H I map of M31, to B. Milliard for the UV (2000 Å) map, and to R. Walterbos for the optical photometry maps. We are indebted to the referee, R. Walterbos, whose comments helped to improve this paper in various aspects. Helpful discussions with C. Beichman, R. Beck, E. Berkhuijsen, J. Fowler, J. Kirk, and J. Lequeux, and useful exchanges with U. Lisenfeld, are acknowledged. Part of the work was done when C. X. was at the Max-Planck-Institut für Radioastronomie, supported by an Alexander von Humboldt Fellowship. He thanks Professor R. Wielebinski for his hospitality. This research is supported in part through the IRAS Extended Mission Program by the Jet Propulsion Laboratory, California Institute of Technology, under a contract with the National Aeronautics and Space Administration. C. X. acknowledges that part of his work in this paper has been done within the framework of the Sonderforschungsberich 328 (Entwicklung von Galaxien) of the Deutsche Forschungsgemeinschaft.

REFERENCES

Allen, R. J., Le Bourlot, J., Lequeux, J., Pineau des Forets, G., & Roueff, E. 1994, preprint
Allen, R. J., & Lequeux, J. 1993, ApJ, 410, L15
Bajaja, E., & Gergeley, T. E. 1977, A&A, 61, 229
Bianchi, L., Hutchings, J. B., & Massey, P. 1991, A&A, 249, 14
Blair, W. P., Kirshner, R. P., & Chevalier, R. A. 1982, ApJ, 254, 50
Boissé, P. 1990, A&A, 228, 483
Boulanger, F., & Péreault, M. 1988, ApJ, 330, 964
Block, D. L., Witt, A. N., Grosbol, P., Stockton, A., & Moneti, A. 1994, A&A, 288, 383
Braun, R. 1991, ApJ, 372, 54
Brinks, E. 1984, Ph.D. thesis, Univ. Leiden
Brinks, E., & Burton, W. B. 1984, A&A, 141, 195
Brinks, E., & Shane, W. W. 1984, A&AS, 55, 179
Buat, V., & Xu, C. 1995, A&A, in press
Burstein, D., Haynes, M. P., & Faber, S. M. 1991, Nature, 353, 515
Burstein, D., & Heiles, C. 1984, ApJS, 54, 33
Byun, Y. I., Freeman, K. C., & Kylafis, N. D. 1994, ApJ, 432, 114
Caplan, J., & Deharveng, L. 1986, A&A, 155, 297
Chini, R., & Krügel, E. 1993, A&A, 166, L8
Cox, P., Krügel, E., & Mezger, P. G. 1986, A&A, 155, 380
Cox, P., & Mezger, P. G. 1989, A&A Rev., 1, 49
Deharveng, J. M., Jakobsen, P., Milliard, B., & Laget, M. 1980, A&A, 88, 52
Désert, F. A., Boulanger, F., & Puget, J. L. 1990, A&A, 273, 215
Deul, E. R. 1989, A&A, 218, 78
Devereux, N. A., & Young, J. S. 1990, ApJ, 359, 42
Disney, M. 1992, Nature, 356, 114
Disney, M., Davies, J., & Phillipps, S. 1989, MNRAS, 239, 939
Draine, B. T., & Anderson, N. 1985, ApJ, 292, 494
Draine, B. T., & Lee, H. M. 1984, ApJ, 285, 89
Emerson, D. T. 1974, MNRAS, 169, 607
Fitzpatrick, E. L. 1986, AJ, 92, 1068
Franceschini, A., & Andreani, P. 1995, ApJ, 440, L5
Helou, G. 1986, ApJ, 311, L33
Hobson, M. P., & Scheuer, P. A. 1993, MNRAS, 264, 145
Hodge, P. 1980, AJ, 85, 376
Hodge, P., & Kennicutt, R. 1982, AJ, 87, 264
Hodge, P., & Lee, M. 1988, ApJ, 329, 651
Holmberg, E. 1958, Medn. Lunds Astr. Obs., 2, 136
Humphreys, M., Bowyer, S., & Martin, C. 1990, AJ, 99, 84
Hutchings, J. B., et al. 1992, ApJ, 400, L35
Israel, F. P., De Boer, K. S., & Bosma, A. 1986, A&AS, 66, 117
Iye, M., & Richter, O. 1985, A&A, 144, 471
Jura, M. 1982, ApJ, 354, 70
Koorneef, J. 1982, A&A, 107, 247
Koper, E. 1993, Ph.D. thesis, Univ. Leiden
Koper, E., Dame, T. M., Israel, F. P., & Thaddeus, P. 1991, ApJ, 383, L11
Kwan, J., & Xie, S. 1992, ApJ, 398, 105
Lonsdale-Persson, C. J., & Helou, G. 1987, ApJ, 314, 513
Mathis, J. S., Mezger, P. G., & Panagia, N. 1983, A&A, 128, 212
Milliard, B. 1984, These, d'Etat, University de Marseille
Rowan-Robinson, M. 1992, MNRAS, 258, 787
Savage, B. D., & Mathis, J. S. 1979, ARA&A, 17, 73
Sofue, Y., & Yoshida, S. 1993, ApJ, 417, L63
Soifer, B. T., Houck, J. R., & Neugebauer, G. 1987, ARA&A, 25, 187
Valentijn, E. A. 1990, Nature, 346, 153
van de Hulst, H. C., & de Jong, T. 1969, Physica, 41, 151
van den Bergh, S. 1975, A&A, 41, 53
———. 1991, PASP, 103, 1053
Walterbos, R. A. M. 1988, in Galactic and Extragalactic Star Formation, ed. R. E. Pudritz & M. Fich (Dordrecht: Kluwer), 361
Walterbos, R. A. M., & Kennicutt, R. C. 1987, A&AS, 69, 311
———. 1988, A&A, 198, 61, (WK88)
Walterbos, R. A. M., & Schwering, P. B. W. 1987, A&A, 180, 27 (WS87)
Xu, C. 1990, ApJ, 365, L47
Xu, C., & Buat, V. 1995, A&A, 293, L65
Xu, C., & De Zotti, G. 1989, A&A, 225, 12
Xu, C., & Helou, G. 1993, in Science with High Spatial Resolution Far-Infrared Data, ed. S. Terebey & J. Mazzarella (Pasadena: Jet Propulsion Laboratory), 87
———. 1994, ApJ, 426, 109
———. 1996, ApJ, 456, 152 (Paper I)